HHS Public Access

Author manuscript

Nat Struct Mol Biol. Author manuscript; available in PMC 2014 February 01.

Published in final edited form as:

Nat Struct Mol Biol. 2013 August ; 20(8): 973–981. doi:10.1038/nsmb.2625.

Initial activation of STIM1, the regulator of store-operated calcium entry

Yubin Zhou[1,3], **Prasanna Srinivasan**[1], **Shiva Razavi**[1], **Sam Seymour**[1], **Paul Meraner**[1], **Aparna Gudlur**[1], **Peter B Stathopulos**[2], **Mitsuhiko Ikura**[2], **Anjana Rao**[1], and **Patrick G Hogan**[1]

[1]La Jolla Institute for Allergy & Immunology, La Jolla, California, USA

[2]Department of Medical Biophysics, University of Toronto, Toronto, Ontario, Canada

Abstract

Physiological Ca^{2+} signalling in T lymphocytes and other cells depends on the STIM-ORAI pathway of store-operated Ca^{2+} entry. STIM1 and STIM2 are Ca^{2+} sensors located in the endoplasmic reticulum (ER) membrane, with ER-luminal domains that monitor cellular Ca^{2+} stores and cytoplasmic domains that gate ORAI channels in the plasma membrane. The STIM ER-luminal domain dimerizes or oligomerizes upon dissociation of Ca^{2+}, but the mechanism transmitting activation to the STIM cytoplasmic domain has not been defined. Here we demonstrate, using Tb^{3+}–acceptor energy transfer, that dimerization of STIM1 ER-luminal domains can initiate an extensive conformational change in murine STIM1 cytoplasmic domains. The conformational change, triggered by apposition of the predicted coiled-coil 1 (CC1) regions, releases the ORAI-activating domains from their interaction with the CC1 regions and allows physical extension of the STIM1 cytoplasmic domain across the gap between ER and plasma membrane to communicate with ORAI channels.

INTRODUCTION

The Ca^{2+} release-activated Ca^{2+} (CRAC) current of T cells and mast cells[1–3] has been a classical example of store-operated Ca^{2+} entry (reviewed in[4]). The classical CRAC current

CORRESPONDENCE: P Hogan, La Jolla Institute for Allergy & Immunology, 9420 Athena Circle, La Jolla, California 92037, USA. TEL 858-952-7175; phogan@liai.org.

[3]Present address: Center for Translational Cancer Research, Institute of Biosciences & Technology, Texas A&M Health Science Center, Houston, Texas, USA

Note: Supplementary information is available on the Nature Structural & Molecular Biology website.

AUTHOR CONTRIBUTIONS

YZ and PGH designed the study. YZ designed engineered proteins and developed the assays, and carried out the experiments with assistance from SR and SS. PS made a detailed study of STIM1 binding to liposomes. PM prepared and characterized liposomes for the binding assays. AG contributed recombinant proteins and technical suggestions. PBS and MI contributed the SEC-MALS characterization of recombinant CC1. YZ, AR, and PGH analyzed data, with input from the other authors. YZ and PGH wrote the manuscript.

COMPETING INTERESTS STATEMENT

AR and PGH are founders of CalciMedica, Inc., and members of its scientific advisory board. The remaining authors state that they have no competing interests.

is triggered by interaction of the ER Ca^{2+} sensor STIM1 with the plasma membrane Ca^{2+} channel ORAI1 (refs. 5–9). Inherited deficits in this pathway in humans and mice lead to immunodeficiency due to impaired function of T effector cells; autoimmune disease due to compromised function of T regulatory cells; and developmental disorders of muscle, skin, teeth, and hair due to altered Ca^{2+} signalling in these tissues (reviewed in[10,11]). There is increasing evidence that the STIM1-ORAI1 pathway and CRAC current also contribute to Ca^{2+} signalling in other cells.

Store-operated Ca^{2+} entry is controlled by the ER-resident Ca^{2+} sensors STIM1 and STIM2 (refs. 5,6,12–16; reviewed in[17–19]). Physiological stimulation— through the T cell receptor, the Fcε receptor of mast cells, or various G protein-coupled receptors in other cells— initiates a sequence of ER Ca^{2+} depletion, dimerization or oligomerization of the STIM luminal domain, and movement of STIM within the ER to sites where ER is closely apposed to plasma membrane (reviewed in[17–19]). The STIM cytoplasmic domain, through its SOAR(CAD) region, then recruits and directly activates the ORAI channel[20–25].

STIM1 at ER-plasma membrane junctions interacts with plasma membrane phosphoinositides, ORAI channels, and other plasma membrane proteins[20–33]. Several of these interactions involve direct physical contact, in which STIM1 and its partner must bridge an ER-plasma membrane separation estimated at 10–25 nm[34–36]. The interaction of a polybasic segment at the very C-terminus of STIM1 with the plasma membrane lipid phosphatidylinositol 4,5-bisphosphate (PIP2)[26–28,37] imposes an important geometric constraint. The PIP2 headgroup is at the cytoplasmic face of the plasma membrane, and hence the cytoplasmic domain of STIM1 must itself bridge the distance from ER to plasma membrane.

To gain insight into the conformational changes in STIM1 that lead to store-operated Ca^{2+} entry, we mapped distances within STIM1 by Tb^{3+}–acceptor energy transfer[38,39]. The lanthanides Tb^{3+} and Eu^{3+} have favorable properties as donor fluorophores for distance measurements, as exemplified, for example, in studies of the protein conformations of myosin, the *Shaker* K^+ channel, and RNA polymerase[40–43]. Moreover, the Tb^{3+} donor and its acceptor can be incorporated into STIM1 as small probes that are unlikely to cause appreciable changes in STIM1 conformations. Experiments described below indicate that the resting STIM1 cytoplasmic domain ($STIM1^{CT}$) in its preferred conformation does not span the > 10 nm separating ER and plasma membrane, implying that $STIM1^{CT}$ undergoes a substantial conformational change upon activation. We characterize this conformational change in biophysical and functional assays, and delineate its mechanism.

RESULTS

"Activating" mutations increase $STIM1^{CT}$ binding to PIP2

Initial targeting of STIM1 to the plasma membrane has been attributed to an interaction of the C-terminal polybasic segment of STIM1 with plasma membrane PIP2 (refs. 26–28,37). We confirmed that $STIM1^{CT}$ binds to PIP2 and phosphatidylinositol 3,4,5-trisphosphate (PIP3) in a commercially available array of seven phosphoinositides, phosphatidylinositol, and certain other common membrane lipids [Figure 1A] and to PIP2 in nanodiscs [Figure

1B; Supplementary Figure 1A], lipoprotein particles in which a belt of engineered apolipoprotein A1 scaffold protein surrounds a small circular lipid bilayer[44].

To dissect the targeting of activated STIM1, we examined the "activated" STIM1 variant L251S, which has been shown to interact more effectively with ORAI1 than wildtype STIM1 (ref. 45). We asked whether it also interacts more strongly with PIP2. We quantitated green fluorescent protein (GFP)-STIM1^{CT} binding to liposomes using an equilibrium dialysis assay, in which binding to PIP2-containing liposomes is reflected in excess fluorescence in the PIP2 chamber over that in the control chamber [Figure 1C; Supplementary Figure 1B–D]. Binding is dependent on the STIM1 polybasic segment, and is modestly increased by the L251S replacement [Figure 1C; Supplementary Figure 1D]. The increased binding correlates with an increased exposure of the C-terminal polybasic segment of STIM1, reported by the environment-sensitive fluorescent probe AEDANS introduced directly adjacent to the polybasic segment [Figure 1D]. Independent measurements of the exposure of the AEDANS fluorophore to collisional quenching of its fluorescence by acrylamide support this conclusion [Supplementary Figure 2A–B].

Among several other STIM1 variants tested, only the activated variant ^{318}EEELE^{322} > AAALA (termed 4EA)[45,46] showed increased exposure of its C-terminal polybasic segment and an increased ability to interact with PIP2 [Supplementary Figures 1D and 2]. However, binding to PIP2 remains weak, suggesting that an additional conformational change or other stabilizing factors contribute to stable STIM1 puncta formation in cells.

"Activating" mutations cause extension of STIM1^{CT}

Wildtype STIM1^{CT} binds PIP2 [Figure 1A–C][28] and ORAI1 (ref. 25) *in vitro*, and the soluble STIM1^{CT} fragment expressed in cells binds and gates ORAI1 channels[20,25,47], posing the question why STIM1 is inactive in resting cells. One hypothesis is that the cytoplasmic domain of STIM1 is retained near the ER until STIM1 is activated.

We utilized Tb^{3+}–acceptor energy transfer[38,39] to measure the distance between STIM1 residue 233, the site at which the cytoplasmic portion of STIM1 emerges from the ER membrane, and the STIM1 C-terminal polybasic tail that interacts with the plasma membrane [Figure 2A]. In the initial experiments, we compared unlabelled wildtype and L251S STIM1^{CT} proteins. The wildtype protein is an elongated dimer that migrates ahead of compact globular proteins of comparable molecular weight on size-exclusion chromatography[25]. The L251S variant migrates slightly ahead of wildtype STIM1^{CT} [Figure 2B; Supplementary Figure 3], reflecting a more extended conformation rather than increased oligomerization, in line with the finding that STIM1(234–491) harboring the L251S replacement is a dimer[45] and with the direct distance measurements below. The circular dichroism (CD) spectrum of L251S variant STIM1^{CT} reports no gross change in secondary structure [Supplementary Figure 3B], but there is a subtle increase in thermal melting at temperatures below 40°C that may reflect loss of an intramolecular interaction that stabilizes a portion of the α-helical secondary structure in the wildtype protein [Figure 2C]. Based on data presented below, it is likely that this is the intramolecular CC1–SOAR(CAD) interaction.

Tb^{3+} was excited through the lanthanide-binding tag (LBT) tryptophan antenna by illumination at 280 nm, and energy transfer from Tb^{3+} to BODIPY™-FL was assessed in emission spectra gated at 200 μs to eliminate scattered light and fluorescence from direct excitation of acceptor. Protein labelled with Tb^{3+} donor alone displays the characteristic narrow Tb^{3+} emission peaks at 490 and 545 nm [Figure 2D]. Protein labelled with both donor and acceptor has, in addition, a broad BODIPY-FL emission peak centered at 515 nm superimposed on the Tb^{3+} peaks [Figure 2D]. Control experiments established that the fluorescence peak at 515 nm is due to Tb^{3+}–BODIPY-FL energy transfer within a $STIM1^{CT}$ dimer [see Supplementary Note].

Decay of Tb^{3+} luminescence in the presence of acceptor is a sensitive test of Tb^{3+}–acceptor energy transfer. LBT-$STIM1^{CT}$ with Tb^{3+} donor alone exhibits a lifetime $\tau \sim 2.32$ ms [Figure 2E], as expected for Tb^{3+} completely shielded from water by coordination to its LBT ligands[48–50]. In wildtype $STIM1^{CT}$ labelled with BODIPY-FL acceptor, Tb^{3+} emission exhibits a major quenched component having a lifetime $\tau \sim 1.21$ ms and a second component having $\tau \sim 0.28$ ms [Figure 2E; Table 1A; Supplementary Table 1]. A third component with $\tau \sim 2.3$ ms represents STIM1 not labelled with acceptor. The sensitized acceptor emission displays components with $\tau \sim 0.98$ ms and $\tau \sim 0.21$ ms [Figure 2E; Table 1A; Supplementary Table 1], in agreement with the quenched donor lifetimes. A straightforward interpretation is that there are two populations of wildtype $STIM1^{CT}$ with different donor–acceptor distances, ~4.2 nm and ~3.0 nm [Table 1A; Supplementary Table 1]. An alternative dynamic interpretation [see Supplementary Note] is that there is a single folded-back conformation with donor–acceptor distance ~3.1 nm, and that the second time constant reflects conformational changes occurring during the excited-state lifetime of Tb^{3+} donor [Table 1B]. In either interpretation, extrapolating to STIM1 in cells, wildtype $STIM1^{CT}$ has a preferred conformation in which the polybasic segment at its C terminus is near the site of STIM1 anchoring in the ER and distant from the plasma membrane.

The gated spectrum of $STIM1^{CT}$ variant L251S labelled with BODIPY-FL shows very little sensitized acceptor signal [Figure 2D], despite efficient labelling with acceptor [Supplementary Figure 3C]. Correspondingly, the donor lifetime in the presence of acceptor is only marginally less than the lifetime of donor alone [Figure 2E; Table 1A; Supplementary Table 1]. To exclude bias introduced by the specific labelling strategy, we made independent measurements on LBT-$STIM1^{CT}$ proteins labelled at the C terminus with a different acceptor fluorophore, BODIPY™-TMR [Supplementary Figure 4A–D; Table 1A; Supplementary Table 1], and on $STIM1^{CT}$ proteins with a C-terminal Tb^{3+} donor and an N-terminal GFP acceptor [Supplementary Figure 4E–G; Table 1; Supplementary Table 1]. In each case, the wildtype donor–acceptor distance is 3–4 nm, and the L251S donor–acceptor distance falls beyond the range that can be estimated confidently with these donor–acceptor pairs, indicating that the distance is increased in the L251S protein by at least 4–5 nm [Figure 2F].

The other "activating" $STIM1^{CT}$ variant, 4EA, also has negligible energy transfer and negligible change in donor lifetime, and thus a large estimated donor–acceptor separation [Supplementary Figure 4H–I; Supplementary Table 1]. Three nonactivating variants of $STIM1^{CT}$ are similar to wildtype $STIM1^{CT}$ in their profiles on size-exclusion

chromatography [Supplementary Figure 3A] and their CD spectra [Supplementary Figure 3B], and do not differ appreciably from wildtype protein in the estimated distances between residue 233 and the polybasic tail [Supplementary Table 1].

CC1–CC1 association induces a conformational change

The CC1 region, STIM1(233–343), is positioned to take part both in bridging the distance between ER and plasma membrane and in propagating an activating conformational change in wildtype $STIM1^{CT}$. There has been a tacit belief that the basal state of CC1 is a coiled coil[51,52], though the primary STIM1 dimerization is through its SOAR(CAD) domain[23,53]. In fact, CC1 in isolation does not assemble as the predicted coiled coil. The molecular mass of the isolated recombinant CC1 fragment, estimated from size-exclusion chromatography coupled with multi-angle light scattering (SEC-MALS), is 12.9 ± 1.1 kDa, comparable to the calculated monomer mass, 14.3 kDa [Figure 3A]. Importantly, the CC1 regions are not closely associated in the context of the dimeric $STIM1^{CT}$ protein, either, as established by a lack of intradimer energy transfer between donor and acceptor probes placed at the N termini of individual monomers within a $STIM1^{CT}$ dimer [Figure 3B–F]. For these experiments, we introduced a HAP2 peptide docking site for fluorescent α-bungarotoxin[54] at the N terminus of $STIM1^{CT}$, coexpressed LBT-$STIM1^{CT}$ and HAP-$STIM1^{CT}$, and purified heterodimers bearing both a donor and an acceptor tag [see Supplementary Note].

This finding led us to explore the hypothesis that bringing CC1 N termini together might trigger a conformational change. We first investigated the secondary structure of the recombinant CC1 monomer and of a CC1 dimer produced by engineering a disulfide bond between the N termini of CC1 monomers [Figure 4A; Supplementary Figure 5A]. CD spectroscopy shows that the CC1 monomer has a modest content of α-helix at 4°C, with a broad melting transition indicative of independent unfolding of parts of CC1 rather than concerted unfolding of a single compact domain [Figure 4B and 4C]. In contrast, the disulfide-linked dimer possesses increased α-helical secondary structure and, tellingly, exhibits a cooperative melting transition at ~60°C, where the monomer is already fully denatured [Figure 4B and 4C]. Thus, physical apposition of the N termini of two CC1 monomers leads to increased CC1–CC1 interactions and a dramatic stabilization of a portion of CC1 secondary structure.

The effect of the L251S replacement casts light on the likely nature of the conformational change. The substitution does not, by itself, affect the thermal melting curve of the CC1 monomer [Figure 4D–F]. However, it prevents the stabilization of α-helical structure by forced dimerization. Given that L251 is in the core of the predicted coiled coil, and taking into account the fractional helix content stabilized, it is likely that the conformational change is formation of a partial coiled coil [Figure 4G].

CC1–CC1 association reduces interaction with SOAR(CAD)

A further key observation is that CC1 dimerization reduces the interaction between CC1 and SOAR(CAD), the minimal ORAI-activating domain within $STIM1^{CT}$. We purified monomeric CC1 and dimeric disulfide-linked CC1, and measured the interaction between these proteins and maltose-binding protein (MBP)-SOAR[53] immobilized on amylose resin.

Comparison of lanes 4 and 6 in [Figure 4H] shows that there is less binding of dimeric CC1 to SOAR(CAD) when equal amounts of CC1 protein are incubated. There is no binding to the MBP negative control [Figure 4H]. These findings are consistent with the hypothesis that bringing the N termini of CC1 into apposition within a $STIM^{CT}$ dimer triggers a conformational change in CC1 and releases SOAR(CAD) from its interaction with CC1, resulting in extension of $STIM^{CT}$.

The replacement L251S in CC1 likewise weakens the interaction between CC1 and MBP-SOAR [Figure 4H]. However, the "activating" mutation L251S and the activating conformational change triggered by CC1–CC1 interaction have a similar effect by different detailed mechanisms. Based on data shown above [Figure 4D–F], the L251S replacement releases SOAR(CAD) without triggering the conformational change in CC1, suggesting that L251 is either part of the CC1–SOAR(CAD) interface in resting $STIM1^{CT}$ or participates in interactions that allosterically stabilize the interface. We propose that the key to STIM1 activation is the release of SOAR(CAD) and the polybasic tail from interactions that tether them near the ER. Active wildtype STIM1 achieves this by sequestering L251 in a CC1–CC1 coiled coil and thereby weakening the interaction with SOAR(CAD). The L251S replacement directly weakens the interaction with SOAR(CAD).

Intradimer CC1–CC1 association causes extension of $STIM1^{CT}$

Finally, we tested whether apposition of the N termini in $STIM1^{CT}$ can initiate a conformational change that propagates throughout $STIM1^{CT}$, using $STIM1^{CT}$ engineered with an LBT at the N terminus and a HAP2 docking site for fluorescent α-bungarotoxin at the C terminus of each monomer [Figure 5A]. An introduced cysteine at the very N terminus was either blocked by reaction with iodoacetamide, to preclude oxidative crosslinking, or intentionally crosslinked with a bifunctional maleimide reagent [Figure 5B; Supplementary Figure 5B]. LBT-$STIM1^{CT}$-HAP2 dimers with the N termini unconstrained recapitulate the energy transfer observed with other wildtype $STIM^{CT}$ proteins, indicating that the protein is in its folded-back conformation [Figure 5C]. In contrast, covalently crosslinked LBT-$STIM1^{CT}$-HAP2 dimers show no energy transfer in the gated spectra and no decrease in the Tb^{3+} luminescence lifetime, reflecting an extended conformation [Figure 5C]. We conclude that apposition of the N termini of CC1 within a $STIM1^{CT}$ dimer triggers a propagating conformational change that results in extension of $STIM1^{CT}$ [Figure 5D].

DISCUSSION

The initial step in STIM1 activation

Our findings have direct implications for the process of STIM1 activation and plasma membrane targeting in cells [Figure 6]. We have established here that CC1 regions do not associate detectably, either in isolation or when attached to SOAR(CAD). The isolated STIM1 ER-luminal domains also do not interact at Ca^{2+} concentrations typical of the ER in resting cells[13,16]. Nevertheless, the STIM1 cytoplasmic domain is clearly dimeric[25], with its primary dimerization through SOAR(CAD)[23]. Therefore we propose that the dimerized SOAR(CAD) regions are connected to the ER in resting cells by two physically independent CC1 tethers. Due to the low density of native STIM1 in the ER, a decrease in luminal Ca^{2+}

will elicit, preferentially, association of the paired luminal domains within a STIM1 dimer. Association of the luminal domains will bring the initial portions of the CC1 regions into apposition, favor an otherwise weak CC1–CC1 interaction, and trigger the physical extension of $STIM1^{CT}$ and the enhanced exposure of the polybasic segment that interacts with PIP2. A similar mechanism is likely to describe activation of STIM2.

The mechanism is roughly the converse of integrin inside-out signalling[55–57]. For integrin αβ dimers, protein-protein interactions at the cytoplasmic face of the plasma membrane, exemplified by talin binding to the integrin β subunit, allow the transmembrane segments of the α and β subunits to move apart, triggering an extension of the integrin extracellular domains and an increase in affinity for physiological integrin ligands. The detailed mechanisms of the STIM and integrin conformational changes are different, and for STIM it remains to be seen whether the transmembrane segments have a specific role other than to connect the luminal and cytoplasmic domains. However, a feature common to STIM1 and integrins is that the conformational change and clustering steps are distinct. In contrast, all previous models for STIM1 activation[15,19,26,45,46,52,53] have posited a single activation step tied to STIM oligomerization.

STIM–STIM FRET changes detected in cells

An increase in STIM–STIM FRET after store depletion was taken to indicate that oligomerization beyond the level of resting STIM1 is the first step in activation[26]. This view was supported by evidence that artificial oligomerization activates STIM[15] and by later STIM–STIM FRET experiments[47,52]. We have defined an activation mechanism that is initiated by the association of paired luminal domains within a preexisting STIM dimer, an association that parallels the dimerization of recombinant STIM1 luminal domains observed in the absence of Ca^{2+} *in vitro*[13,16]. It is reasonable to ask whether there is a correlate in the cellular experiments. Is luminal dimer formation temporally separable in the cellular assays from higher-order oligomerization? Is it even detectable?

It can be argued that luminal domain dimerization has gone undetected in cellular studies of full-length STIM1. Covington *et al*. showed, using a STIM protein (STIM1-ΔC) consisting of only the luminal domain and transmembrane segment, that the luminal domain alone cannot drive oligomerization to the extent observed with full-length STIM1 (ref. 52). The very small FRET signal from STIM1-ΔC at rest in those experiments could plausibly come from luminal domain monomers, with the larger signal after store depletion reflecting the formation of luminal domain dimers. In this view, since the FRET signal from CFP- and YFP-labelled full-length STIM at rest is already comparable to the signal from STIM1-ΔC luminal domain dimers after store depletion, the initial step of luminal domain association could be silent. Then the first step detected by FRET would be SOAR(CAD)-dependent oligomerization.

The high resting FRET signal in the case of full-length STIM1 deserves comment, because it has two interpretations, which lead to different conclusions about the configuration of unlabelled STIM1. In the first possibility, FRET between CFP- and YFP-labelled STIM proteins in resting cells accurately reflects proximity of the transmembrane segments of the unlabelled STIM dimer in resting cells. This possibility must be taken seriously, since the

very pronounced conservation of the STIM1 transmembrane region across vertebrates could well indicate preservation of a sequence that allows a specific local rearrangement during activation. However, since we find that the two N termini of $STIM1^{CT}$ dimers in solution are well separated, this interpretation implies that there is an unidentified geometric constraint on full-length STIM1 in cells that does not apply to the isolated $STIM1^{CT}$ dimers. The second possibility is that the CFP and YFP labels in labelled STIM1 are appreciably closer together than are the transmembrane segments of the unlabelled STIM dimer. In that case, store depletion would induce both a substantial relative movement of the luminal domains and SOAR(CAD)-dependent oligomerization in unmodified wildtype STIM1. Both possibilities are represented in Figure 6.

CC1–CC1 interaction

Covington *et al*. also documented a CC1–CC1 interaction in an engineered STIM1 protein truncated after CC1 (STIM1-CC1)[52]. The protein-protein interaction was weak, in agreement with our observations on isolated CC1, stabilizing luminal domain dimers for immunoprecipitation only in conditions of low Ca^{2+} and low ionic strength buffer. Yet, somewhat surprisingly, FRET measurements indicated that the interaction resulted in dimerization of the luminal domains in resting cells[52]. Whereas Covington *et al*. took this as evidence that CC1 supports the formation of inactive STIM1 oligomers in resting cells, we attribute the CC1-based dimerization in cells to the heightened CC1–CC1 interactions of overexpressed STIM1-CC1 confined to the ER membrane and the absence of competition from SOAR(CAD). Indeed, since loss of Ca^{2+} favors CC1–CC1 interaction, the converse is true as well, and may shift the Ca^{2+} dependence of monomer-dimer equilibrium so that the luminal domains of STIM1-CC1 are present as the Ca^{2+}-free dimer even prior to store depletion.

Earlier views of the activating conformational change

Korzeniowski *et al*. pioneered the study of activating mutations in the STIM1 cytoplasmic domain with a demonstration that the 4EA (^{318}EEELE^{322} > AAALA) variant of STIM1 is constitutively active[46]. They found further that artificial recruitment of a long CC1 fragment containing the EEELE sequence, STIM1(238–343), to the plasma membrane inhibited STIM-ORAI communication in a fraction of cells. Based on these data, they suggested that the acidic sequence interacts under resting conditions with a basic segment of $STIM1^{CT}$, thus masking the ORAI-interacting SOAR(CAD), and that STIM oligomerization unmasks SOAR(CAD). The specific interaction proposed is at variance with subsequently published structural evidence[53] and with the failure of the ^{382}KIKKK^{386} > QIQQQ mutant to cause extension of $STIM1^{CT}$ in the current study, but the notion that STIM oligomerization unmasks SOAR(CAD) has continued to resonate.

Muik *et al*. characterized further mutations in CC1 and SOAR(CAD), assessed in the context of STIM1(233–474), which they termed ORAI1 activating small fragment or OASF[45]. Several of these mutations caused a reduction in the FRET signal from a CFP-OASF-YFP protein, indicating that the mutated OASF proteins assume a more extended conformation than wildtype OASF. The conformational change correlated with activation of STIM1 in cases selected for examination, because the mutant OASF proteins displayed

increased binding to ORAI1, and because introduction of the substitutions into into full-length STIM1 led to constitutive activation of ORAI1. Based on these findings, Muik *et al*. proposed that physiological activation of STIM1 triggers oligomerization and conversion of the STIM1 cytoplasmic domain to an extended form, but did not address the mechanism linking oligomerization and conformational change. The most potent single-residue changes identified in the FRET assay were substitutions at L251 or at L248, a neighboring residue predicted to be in the CC1 core, providing the first evidence that the initial region of CC1 is a determinant of the STIM1 resting conformation.

The recently published structure of a portion of *Caenorhabditis elegans* STIM-1 cytoplasmic domain (PDB ID: 3TER) shows an α-helix spanning *C elegans* STIM-1 residues 260–276 folded back against the SOAR domain[53]. This short segment, which corresponds to human STIM1 residues 318–334, was designated the inhibitory helix, though experimental support for the designation is limited to the activated phenotype of the human 4EA variant[46] and of a variant produced by aggressive deletion of human STIM1 residues 310–337 (ref. 53). This interpretation of the structure led to a model in which store depletion causes the STIM1 luminal domain to dimerize or oligomerize, bringing about conformational changes in the inhibitory helices and release of SOAR(CAD). This proposal is more specific than the model of Muik *et al*., but, in focusing on the inhibitory helix, it is likely to reflect only one part of the CC1–SOAR interaction. First, *C elegans* CC1 is considerably shorter than mammalian CC1, and the part of *C elegans* CC1 that is resolved in the crystal structure comprises only the 27 residues immediately N-terminal to SOAR. Thus, a stretch of more than 80 residues of mammalian STIM1 CC1 is not represented, including an extensive region flanking L251. Second, the human ^{318}EEELE^{322} segment is present in the structure as *C elegans* ^{260}HTEME^{264}, but, of these residues, only E264 is seen to make contact with SOAR(CAD). Most tellingly, the presence of the “inhibitory helix” is not sufficient to maintain mammalian STIM1 in its inactive state, since STIM1(315–462) is fully active[46], as is full-length STIM1 with the L251S substitution[45].

With our study, these proposals can be updated to incorporate a concrete mechanism in which luminal domain association leads to CC1–CC1 association and to release of SOAR(CAD) and the STIM1 polybasic tail. Although the precise configuration of CC1 in the inactive STIM1 cytoplasmic domain remains to be defined, it seems likely that CC1 is folded against SOAR(CAD), with several regions including the segment around residues L248 and L251 contributing to maintenance of the inactive conformation. Our data suggest that CC1 redeploys upon activation as an extended α-helical structure with at least its N-terminal portion forming a coiled coil.

Conclusion

We have shown here that a key step in physiological activation of STIM1 is a conformational change that enables STIM1 to bridge the distance from ER to plasma membrane where it can engage PIP2 and ORAI. The conformational change arises from the association of STIM1 ER-luminal domains, and is independent of subsequent STIM oligomerization. Since this conformational rearrangement of the STIM1 dimer involves only two STIM1 Ca^{2+}-binding sites, the steep cooperativity of physiological STIM1

activation[14,15] must depend on further oligomerization following the initial activation step. It remains to be determined how higher-order STIM oligomerization is facilitated by the high local density of STIM1 at ER-plasma membrane junctions, by partner proteins, and by binding to plasma membrane lipids or ORAI.

METHODS

Methods and any associasted references are available in the online version of the paper at http://www.nature.com/nsmb/

ONLINE METHODS

Engineered proteins

STIM1^{CT}, its fragments CC1, SOAR(CAD) (as the MBP-SOAR fusion protein[53]), and STIM1^{CT}-ΔK, STIM1 variants, and GFP-STIM1^{CT} variants were expressed in *E. coli* and purified using standard techniques. Short lanthanide-binding tag (LBT)[58] or HAP tag[54] sequences were inserted into the proteins as indicated, for labelling, respectively, with Tb^{3+} as donor fluorophore or with α-bungarotoxin carrying an acceptor fluorophore. Cysteine residues for covalent labelling or for crosslinking were engineered into cysteine-less STIM1^{CT}(C437S) or into the CC1 fragment, and fluorescent labels were incorporated as indicated. The recombinant proteins were characterized by FPLC, CD spectroscopy, SEC-MALS, and reducing and nonreducing SDS-polycrylamide gel electrophoresis.

Fluorescence spectroscopy

Fluorescence spectra and emission decay measurements were acquired using a QM40 spectrofluorometer (Photon Technology International). Tb^{3+} luminescence and Tb^{3+}-sensitized acceptor emission were excited at 280 nm, and AEDANS fluorescence at 335 nm. Gated fluorescence spectra and emission decay measurements utilized a pulsed xenon excitation source. The decay of Tb^{3+} emission was monitored at 490 nm or at 545 nm, and the decay of acceptor emission at 515 nm or at 570 nm, as appropriate. Data collection was from 200 μs to 10 ms, and 3000 shots were averaged. Protein concentration in the Tb^{3+}–acceptor energy transfer experiments was below 300 nM and the measurements were made at 4 °C in buffer containing 80% glycerol to avoid diffusion-enhanced energy transfer to bystander molecules [Supplementary Figure 6D–E].

Distance estimates

Emission decay curves were fitted to a sum of one, two, or three exponentials using Felix GX software supplied with the spectrofluorometer. Energy transfer efficiency E and donor–acceptor distance R were calculated using the equations for Förster energy transfer[39]. Since each STIM1^{CT} protein for which energy transfer was observed yielded two distinct decay constants corresponding to Tb^{3+}–acceptor energy transfer, this conventional treatment resulted in two distance estimates for each case, and an estimate of the relative occupancies of the corresponding conformations. Although there is no compelling evidence that a fraction of wildtype STIM1^{CT} can assume an extended conformation in which there is no energy transfer, the negligible energy transfer in the L251S variant establishes the existence

of such an extended conformation in activated forms of STIM1. Hence the data were also fitted to an alternative model with a single conformation exhibiting energy transfer, an extended conformation in which there is no energy transfer, and exchange between the two conformations during the lifetime of excited Tb^{3+}. Details are provided in the Supplementary Note. This fitting procedure results in estimates of a single donor–acceptor distance, a rate of exchange between the conformations, and the relative occupancies of the two conformations in equilibrium.

STIM1-PIP2 binding

For the nanodisc binding assay, membrane scaffold protein 1D1 (MSP1D1) was purified and assembled into nanodiscs with 1,2-dimyristoyl-*sn*-glycero-3-phosphocholine (DMPC)[60]. The fluorescent lipid 1,2-dioleoyl-*sn*-glycero-3-phosphoethanolamine-N-(carboxyfluorescein) (PE-CF) was incorporated into the nanodiscs as donor fluorophore. In control nanodiscs, the DMPC:PE-CF ratio was 79:1. In nanodiscs containing PIP2, the DMPC:PE-CF:PIP2 ratio was 79:1:2. $STIM1^{CT}$-TMR was titrated into a nanodisc sample at concentrations up to 2 μM, and STIM1–nanodisc binding was monitored by measurements of PE-CF-sensitized TMR fluorescence emission, with excitation at 450 nm to minimize direct excitation of acceptor.

Binding of GFP-$STIM1^{CT}$ to PIP2-containing liposomes was assessed quantitatively in a two-chamber microdialysis assay. Control liposomes consisted of 1-palmitoyl-2-oleoyl-*sn*-glycero-3-phosphocholine (POPC), 1-palmitoyl-2-oleoyl-*sn*-glycero-3-phospho-L-serine (POPS), and 1-palmitoyl-2-oleoyl-*sn*-glycero-3-phosphoethanolamine (POPE) in a 4:1:2 molar ratio. PIP2 liposomes contained additionally 2 mol% PIP2 unless a different PIP2 content is specified. For the assay, a microdialysis cell of 200 μL total capacity was divided into two equal chambers by a cellulose acetate membrane, with nominal molecular weight cutoff 300 kDa, permeable to GFP-$STIM1^{CT}$ but not to the substantially larger liposomes. The cell was loaded initially with PIP2 liposomes and GFP-$STIM1^{CT}$ or the indicated GFP-$STIM1^{CT}$ variant (10 nM) in one dialysis chamber, and with control liposomes and the same protein at the same concentration in the other chamber. After equilibration, GFP fluorescence was determined in samples recovered from each chamber, corrected for the scattering signal due to the liposomes, and the fraction of GFP-$STIM1^{CT}$ bound was calculated as $(F_{PIP2} - F_{control})/ (F_{control} + F_{PIP2})$, where F_{PIP2} is the fluorescence intensity in the chamber with PIP2 liposomes and $F_{control}$ is the fluorescence intensity in the control chamber.

CC1–SOAR(CAD) interaction

MBP or MBP-SOAR was immobilized on amylose resin, incubated for 4 h at 4°C with 400 μg of the recombinant CC1 protein indicated, and washed extensively. Bound protein was analyzed by nonreducing SDS-polyacrylamide gel electrophoresis. Protein bands stained with Coomassie Brilliant Blue R-250 were quantitated using the program ImageJ (National Institute of Mental Health).

Data analysis and statistics

Error bars indicate mean ± s.e.m., except in the case of CC1(L251S) in Figure 4H, where they indicate the range. Because fitted lifetimes need not be distributed according to a Gaussian function, mean values are reported in Table 1A without an attempt to estimate statistical variability, and the actual fitted values from all experiments are reported in Supplementary Figure 1A.

Supplementary Material

Refer to Web version on PubMed Central for supplementary material.

ACKNOWLEDGMENTS

This work was funded by US National Institutes of Health grants AI084167 and AI40127 (to AR and PGH) and by grants from the Canadian Institutes of Health Research and the Heart and Stroke Foundation of Canada (to MI). YZ has been supported by a postdoctoral fellowship from The Leukemia & Lymphoma Society and by an LLS Special Fellow award, P Srinivasan by a Human Frontier Science Program cross-disciplinary fellowship, and AG by a Cancer Research Institute-Irvington Institute Fellowship. We thank Y. Shen (Nankai University, Tianjin, China) for the plasmid pMCSG9-SOAR and S. Sligar (University of Illinois Urbana-Champaign, Urbana, IL, USA) for the plasmid pMSP1D1.

REFERENCES

1. Hoth M, Penner R. Depletion of intracellular calcium stores activates a calcium current in mast cells. Nature. 1992; 355:353–356. [PubMed: 1309940]
2. Hoth M, Penner R. Calcium release-activated calcium current in rat mast cells. J. Physiol. 1993; 465:359–386. [PubMed: 8229840]
3. Zweifach A, Lewis RS. Mitogen-regulated Ca^{2+} current of T lymphocytes is activated by depletion of intracellular Ca^{2+} stores. Proc. Natl. Acad. Sci. USA. 1993; 90:6295–6299. [PubMed: 8392195]
4. Parekh AB, Putney JW Jr. Store-operated calcium channels. Physiol. Rev. 2005; 85:757–810. [PubMed: 15788710]
5. Roos J, DiGregorio PJ, Yeromin AV, Ohlsen K, Lioudyno M, Zhang S, Safrina O, Kozak JA, Wagner SL, Cahalan MD, Veliçelebi G, Stauderman KA. STIM1, an essential and conserved component of store-operated Ca^{2+} channel function. J. Cell Biol. 2005; 169:435–445. [PubMed: 15866891]
6. Liou J, Kim ML, Heo WD, Jones JT, Myers JW, Ferrell JE, Meyer T Jr. STIM is a Ca^{2+} sensor essential for Ca^{2+} -store-depletion-triggered Ca^{2+} influx. Curr Biol. 2005; 15:1235–1241. [PubMed: 16005298]
7. Feske S, Gwack Y, Prakriya M, Srikanth S, Puppel SH, Tanasa B, Hogan PG, Lewis RS, Daly M, Rao A. A mutation in Orai1 causes immune deficiency by abrogating CRAC channel function. Nature. 2006; 441:179–185. [PubMed: 16582901]
8. Vig M, Peinelt C, Beck A, Koomoa DL, Rabah D, Koblan-Huberson M, Kraft S, Turner H, Fleig A, Penner R, Kinet JP. CRACM1 is a plasma membrane protein essential for store-operated Ca^{2+} entry. Science. 2006; 312:1220–1223. [PubMed: 16645049]
9. Zhang SL, Yeromin AV, Zhang XH, Yu Y, Safrina O, Penna A, Roos J, Stauderman KA, Cahalan MD. Genome-wide RNAi screen of Ca^{2+} influx identifies genes that regulate Ca^{2+} release-activated Ca^{2+} channel activity. Proc. Natl. Acad. Sci. USA. 2006; 103:9357–9362. [PubMed: 16751269]
10. Feske S. ORAI1 and STIM1 deficiency in human and mice: roles of store-operated Ca^{2+} entry in the immune system and beyond. Immunol. Rev. 2009; 231:189–209. [PubMed: 19754898]
11. Feske S. Immunodeficiency due to defects in store-operated calcium entry. Ann. N. Y. Acad. Sci. 2011; 1238:74–90. [PubMed: 22129055]

12. Zhang SL, Yu Y, Roos J, Kozak JA, Deerinck TJ, Ellisman MH, Stauderman KA, Cahalan MD. STIM1 is a Ca^{2+} sensor that activates CRAC channels and migrates from the Ca^{2+} store to the plasma membrane. Nature. 2005; 437:902–905. [PubMed: 16208375]
13. Stathopulos PB, Li GY, Plevin MJ, Ames JB, Ikura M. Stored Ca2+ depletion-induced oligomerization of stromal interaction molecule 1 (STIM1) via the EF-SAM region: An initiation mechanism for capacitative Ca^{2+} entry. J. Biol. Chem. 2006; 281:35855–35862. [PubMed: 17020874]
14. Brandman O, Liou J, Park WS, Meyer T. STIM2 is a feedback regulator that stabilizes basal cytosolic and endoplasmic reticulum Ca^{2+} levels. Cell. 2007; 131:1327–1339. [PubMed: 18160041]
15. Luik R, Wang B, Prakriya M, Wu MM, Lewis RS. Oligomerization of STIM1 couples ER calcium depletion to CRAC channel activation. Nature. 2008; 454:538–542. [PubMed: 18596693]
16. Stathopulos PB, Zheng L, Li GY, Plevin MJ, Ikura M. Structural and mechanistic insights into STIM1-mediated initiation of store-operated calcium entry. Cell. 2008; 135:110–122. [PubMed: 18854159]
17. Cahalan MD. STIMulating store-operated Ca^{2+} entry. Nat. Cell Biol. 2009; 11:669–677. [PubMed: 19488056]
18. Hogan PG, Lewis RS, Rao A. Molecular basis of calcium signaling in lymphocytes: STIM and ORAI. Annu. Rev. Immunol. 2010; 28:491–533. [PubMed: 20307213]
19. Soboloff J, Rothberg BS, Madesh M, Gill DL. STIM proteins: dynamic calcium signal transducers. Nat. Rev. Mol. Cell Biol. 2012; 13:549–565. [PubMed: 22914293]
20. Huang GN, Zeng W, Kim JY, Yuan JP, Han L, Muallem S, Worley PF. STIM1 carboxyl-terminus activates native SOC, I^{crac} and TRPC1 channels. Nat. Cell Biol. 2006; 8:1003–1010. [PubMed: 16906149]
21. Yuan JP, Zeng W, Dorwart MR, Choi YJ, Worley PF, Muallem S. SOAR and the polybasic STIM1 domains gate and regulate Orai channels. Nat. Cell Biol. 2009; 11:337–343. [PubMed: 19182790]
22. Park CY, Hoover PJ, Mullins FM, Bachhawat P, Covington ED, Raunser S, Walz T, Garcia KC, Dolmetsch RE, Lewis RS. STIM1 clusters and activates CRAC channels via direct binding of a cytosolic domain to Orai1. Cell. 2009; 136:876–890. [PubMed: 19249086]
23. Muik M, Fahrner M, Derler I, Schindl R, Bergsmann J, Frischauf I, Groschner K, Romanin C. A cytosolic homomerization and a modulatory domain within STIM1 C terminus determine coupling to ORAI1 channels. J. Biol. Chem. 2009; 284:8421–8426. [PubMed: 19189966]
24. Kawasaki T, Lange I, Feske S. A minimal regulatory domain in the C terminus of STIM1 binds to and activates ORAI1 CRAC channels. Biochem. Biophys. Res. Commun. 2009; 385:49–54. [PubMed: 19433061]
25. Zhou Y, Meraner P, Kwon HT, Machnes D, Oh-hora M, Zimmer J, Huang Y, Stura A, Rao A, Hogan PG. STIM1 gates the store-operated calcium channel ORAI1 *in vitro* . Nat. Struct. Mol. Biol. 2010; 17:112–116. [PubMed: 20037597]
26. Liou J, Fivaz M, Inoue T, Meyer T. Live-cell imaging reveals sequential oligomerization and local plasma membrane targeting of stromal interaction molecule 1 after Ca2+ store depletion. Proc. Natl. Acad. Sci. USA. 2007; 104:9301–9306. [PubMed: 17517596]
27. Walsh CM, Chvanov M, Haynes LP, Petersen OH, Tepikin AV, Burgoyne RD. Role of phosphoinositides in STIM1 dynamics and store-operated calcium entry. Biochem. J. 2009; 425:159–168. [PubMed: 19843011]
28. Ercan E, Momburg F, Engel U, Temmerman K, Nickel W, Seedorf M. A conserved, lipidmediated sorting mechanism of yeast Ist2 and mammalian STIM proteins to the peripheral ER. Traffic. 2009; 10:1802–1818. [PubMed: 19845919]
29. Frischauf I, Muik M, Derler I, Bergsmann J, Fahrner M, Schindl R, Groschner K, Romanin C. Molecular determinants of the coupling between STIM1 and Orai channels: differential activation of Orai1–3 channels by a STIM1 coiled-coil mutant. J. Biol. Chem. 2009; 284:21696–21706. [PubMed: 19506081]

30. Zeng Y, Yuan JP, Kim MS, Choi YJ, Huang GN, Worley PF, Muallem S. STIM1 gates TRPC channels, but not Orai1, by electrostatic interaction. Mol. Cell. 2008; 32:439–448. [PubMed: 18995841]

31. Lefkimmiatis K, Srikanthan M, Maiellaro I, Moyer MP, Curci S, Hofer AM. Store-operated cyclic AMP signalling mediated by STIM1. Nat. Cell Biol. 2009; 11:433–442. [PubMed: 19287379]

32. Park CY, Shcheglovitov A, Dolmetsch R. The CRAC channel activator STIM1 binds and inhibits L-type voltage-gated calcium channels. Science. 2010; 330:101–105. [PubMed: 20929812]

33. Wang Y, Deng X, Mancarella S, Hendron E, Eguchi S, Soboloff J, Tang XD, Gill DL. The calcium store sensor, STIM1, reciprocally controls Orai and $Ca_V1.2$ channels. Science. 2010; 330:105–109. [PubMed: 20929813]

34. Wu MM, Buchanan J, Luik RM, Lewis RS. Ca^{2+} store depletion causes STIM1 to accumulate in ER regions closely associated with the plasma membrane. J. Cell Biol. 2006; 174:803–813. [PubMed: 16966422]

35. Várnai P, Tóth B, Tóth DJ, Hunyady L, Balla T. Visualization and manipulation of plasma membrane-reticulum contact sites indicates the presence of additional molecular components within the STIM1-Orai1 complex. J. Biol. Chem. 2007; 282:29678–29690. [PubMed: 17684017]

36. Orci L, Ravazzola M, Le Coadic M, Shen WW, Demaurex N, Cosson P. STIM1-induced precortical and cortical subdomains of the endoplasmic reticulum. Proc. Natl. Acad. Sci. USA. 2009; 106:19358–19362. [PubMed: 19906989]

37. Carrasco S, Meyer T. STIM proteins and the endoplasmic reticulum-plasma membrane junctions. Annu. Rev. Biochem. 2011; 80:973–1000. [PubMed: 21548779]

38. Selvin PR, Hearst JE. Luminescence energy transfer using a terbium chelate: improvements on fluorescence energy transfer. Proc. Natl. Acad. Sci. USA. 1994; 91:10024–10028. [PubMed: 7937831]

39. Selvin PR. Principles and biophysical applications of lanthanide-based probes. Annu. Rev. Biophys. Biomol. Struct. 2002; 31:275–302. [PubMed: 11988471]

40. Xiao M, Reifenberger JG, Wells AL, Baldacchino C, Chen LQ, Ge P, Sweeney HL, Selvin PR. Struct. Nat. Struct. Biol. 2003; 10:402–408. [PubMed: 12679807]

41. Cha A, Snyder GE, Selvin PR, Bezanilla F. Atomic scale movement of the voltage-sensing region in a potassium channel measured via spectroscopy. Nature. 1999; 402:809–813. [PubMed: 10617201]

42. Posson DJ, Ge P, Miller C, Bezanilla F, Selvin PR. Small vertical movement of a K^+ channel voltage sensor measured with luminescence energy transfer. Nature. 2005; 436:848–851. [PubMed: 16094368]

43. Callaci S, Heyduk E, Heyduk T. Core RNA polymerase from E. coli induces a major change in the domain arrangement of the σ^{70} subunit. Mol. Cell. 1999; 3:229–238. [PubMed: 10078205]

44. Nath A, Atkins WM, Sligar SG. Applications of phospholipid bilayer nanodiscs in the study of membranes and membrane proteins. Biochemistry. 2007; 46:2059–2069. [PubMed: 17263563]

45. Muik M, Fahrner M, Schindl R, Stathopulos P, Frischauf I, Derler I, Plenk P, Lackner B, Groschner K, Ikura M, Romanin C. STIM1 couples to ORAI1 via an intramolecular transition into an extended conformation. EMBO J. 2011; 30:1678–1689. [PubMed: 21427704]

46. Korzeniowski MK, Manjarrés IM, Várnai P, Balla T. Activation of STIM1-Orai1 involves an intramolecular switching mechanism. Sci. Signal. 2010; 3(148) ra82.

47. Muik M, Frischauf I, Derler I, Fahrner M, Bergsmann J, Eder P, Schindl R, Hesch C, Polzinger B, Fritsch R, Kahr H, Madl J, Gruber H, Groschner K, Romanin C. Dynamic coupling of the putative coiled-coil domain of ORAI1 with STIM1 mediates ORAI1 channel activation. J. Biol. Chem. 2008; 283:8014–8022. [PubMed: 18187424]

48. Horrocks WD, Sudnick DR Jr. Lanthanide ion probes of structure in biology. Laser-induced luminescence decay constants provide a direct measure of the number of metal-coordinated water molecules. J. Am. Chem. Soc. 1979; 101:334–340.

49. Beeby A, Clarkson IM, Dickins RS, Faulkner S, Parker D, Royle L, de Sousa AS, Gareth Williams JA, Woods M. Non-radiative deactivation of the excited states of europium, terbium and ytterbium complexes by proximate energy-matched OH, NH and CH oscillators: an improved luminescence method for establishing solution hydration states. J. Chem. Soc. Perkin Trans. 1999; 2:493–503.

50. Martin, L. Development of lanthanide-binding tags (LBTs) as powerful and versatile peptides for use in studies of proteins and protein interactions. Cambridge, Massachusetts, USA: Dissertation, Massachusetts Institute of Technology; 2008.
51. Williams RT, Manji SS, Parker NJ, Hancock MS, Van Stekelenburg L, Eid JP, Senior PV, Kazenwadel JS, Shandala T, Saint R, Smith PJ, Dziadek MA. Identification and characterization of the STIM (stromal interaction molecule) gene family: coding for a novel class of transmembrane proteins. Biochem J. 2001; 357:673–685. [PubMed: 11463338]
52. Covington ED, Wu MM, Lewis RS. Essential role for the CRAC activation domain in store-dependent oligomerization of STIM1. Mol. Biol. Cell. 2010; 21:1897–1907. [PubMed: 20375143]
53. Yang X, Jin H, Cai X, Li S, Shen Y. Structural and mechanistic insights into the activation of Stromal interaction molecule 1 (STIM1). Proc. Natl. Acad. Sci. USA. 2012; 109:5657–5662. [PubMed: 22451904]
54. Katchalski-Katzir E, Kasher R, Balass M, Scherf T, Harel M, Fridkin M, Sussman JL, Fuchs S. Design and synthesis of peptides that bind alpha-bungarotoxin with high affinity and mimic the three-dimensional structure of the binding-site of acetylcholine receptor. Biophys. Chem. 2003; 100:293–305. [PubMed: 12646372]
55. Lau T-Y, Kim C, Ginsberg MH, Ulmer TS. The structure of the integrin αIIbβ3 transmembrane complex explains integrin transmembrane signalling. EMBO J. 2009; 28:1351–1361. [PubMed: 19279667]
56. Anthis NJ, Wegener KL, Ye F, Kim C, Goult BT, Lowe ED, Vakonakis I, Bate N, Critchley DR, Ginsberg MH, Campbell ID. The structure of an integrin talin complex reveals the basis of inside-out signal transduction. EMBO J. 2009; 28:3623–3632. [PubMed: 19798053]
57. Kim C, Ye F, Ginsberg MH. Regulation of integrin activation. Annu. Rev. Cell Dev. Biol. 2011; 27:321–345. [PubMed: 21663444]
58. Sculimbrene BR, Imperiali B. Lanthanide-binding tags as luminescent probes for studying protein interactions. J. Am. Chem. Soc. 2006; 128:7346–7352. [PubMed: 16734490]
59. Heyduk T, Heyduk E. Luminescence energy transfer with lanthanide chelates: interpretation of sensitized acceptor decay amplitudes. Anal. Biochem. 2001; 289:60–67. [PubMed: 11161295]
60. Ritchie TK, Grinkova YV, Bayburt TH, Denisov IG, Zolnerciks JK, Atkins WM, Sligar SG. Chapter 11 - Reconstitution of membrane proteins in phospholipid bilayer nanodiscs. Methods Enzymol. 2009; 464:211–231. [PubMed: 19903557]

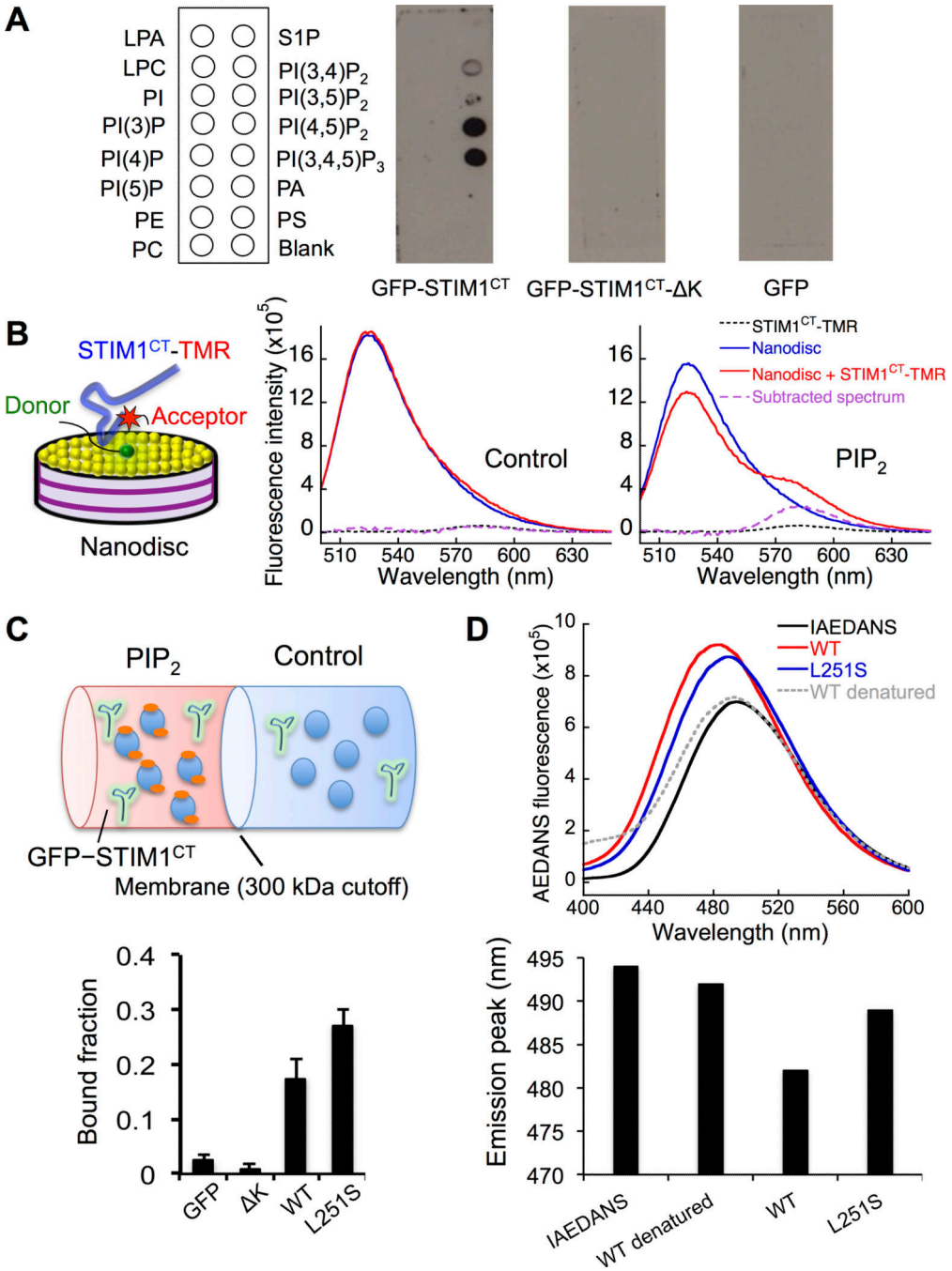

Figure 1. STIM1-PIP2 interaction

(A) GFP-STIM1^{CT} binding to PIP2 and other lipids arrayed on a lipid strip. GFP-STIM1^{CT} lacking the C-terminal polybasic segment (GFP-STIM1^{CT}-ΔK) and GFP alone are controls. (B) GFP-STIM1^{CT} binding to nanodiscs. *Left*, schematic of the experiment. A fluorescent phospholipid analog (1,2-dioleoyl-*sn*-glycero-3-phosphoethanolamine-N-(carboxyfluorescein)) serves as donor, and tetramethylrhodamine (TMR) attached to STIM1^{CT} as acceptor. *Center* and *right*, binding measurements on control and PIP2-containing nanodiscs. Recorded spectra are for nanodiscs alone (*green*), nanodiscs together

with STIM1^{CT} (*red*), and STIM1^{CT} alone (*black*). In the subtracted spectra (*lavender*), donor fluorescence has been removed from the nanodisc + STIM1^{CT} spectra by subtracting an appropriately scaled nanodisc-alone spectrum. Only nanodiscs containing PIP2 exhibit energy transfer (*right panel*, compare *lavender curve* with *black curve*) confirming the specific association of GFP-STIM1^{CT} with PIP2 in bilayers.

(C) GFP-STIM1^{CT} binding to liposomes. *Upper*, schematic of the equilibrium dialysis experiment. One chamber was loaded with PIP2-containing liposomes, the other chamber with control liposomes. The initial concentration of STIM1^{CT} in the two chambers was identical. *Lower*, the excess of GFP-STIM1^{CT} recovered from the PIP2 chamber after equilibration, as a fraction of total GFP-STIM1^{CT} in both chambers.

(D) Exposure of the STIM1^{CT} C terminus assessed with an environment-sensitive probe. *Upper*, fluorescence spectra of IAEDANS and of AEDANS covalently attached to the indicated STIM1^{CT} proteins at introduced residue cysteine-686. *Lower*, wavelengths of peak fluorescence emission. The shift of the peak to a shorter wavelength in the wildtype protein reports partial burial of the fluorophore. Representative of two experiments.

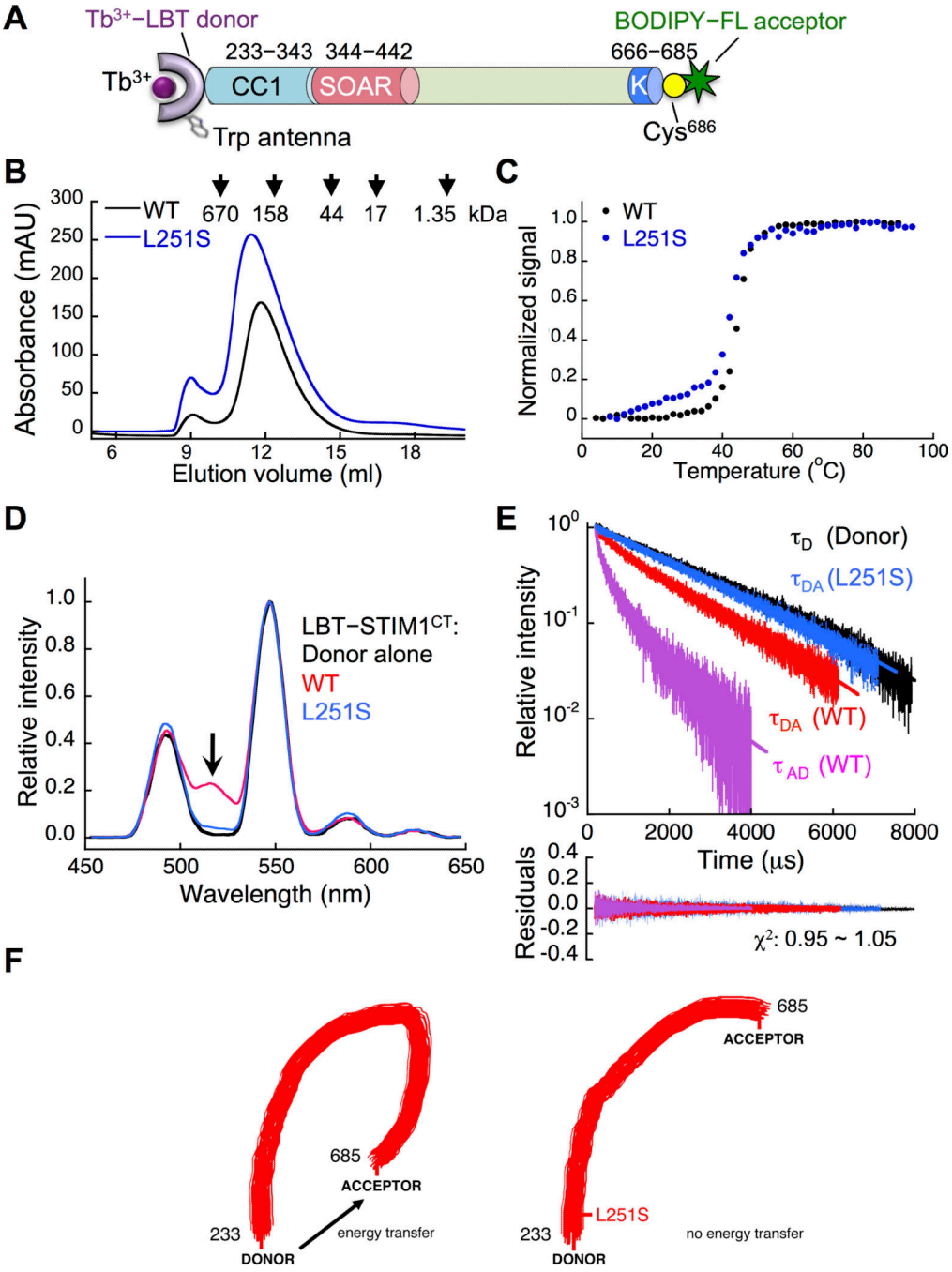

Figure 2. Distance measurements in STIM1 cytoplasmic domain

(A) Schematic of STIM1^{CT} donor–acceptor labelling. STIM1^{CT}(C437S) was engineered with a lanthanide-binding tag (LBT)[58] at its N terminus for labelling with donor Tb^{3+} and an added cysteine residue at its C terminus for labelling with acceptor fluorophore [see also Supplementary Figure 6]. The LBT is an engineered EF-hand with high affinity for Tb^{3+} and with a tryptophan residue positioned to serve as an antenna for excitation of Tb^{3+}. The sequence of murine STIM1^{CT} used in these experiments is closely similar to human STIM1^{CT} throughout, and in particular is identical in CC1 and differs by a single K371R

substitution in SOAR(CAD). CC1, predicted coiled coil region 1; SOAR, STIM1 Orai activating region; K, C-terminal polybasic tail.

(B) Size-exclusion chromatography of wildtype and L251S variant $STIM1^{CT}$ proteins.

(C) Thermal melting monitored as change in circular dichroism at 222 nm. High-resolution thermal melting measurements detect a difference in stability between wildtype $STIM1^{CT}$ and the activated variant L251S at temperatures below 40°C.

(D) Gated luminescence spectra of labelled $STIM1^{CT}$ proteins. The spectra were collected after 200 μs to eliminate light scattering and directly excited acceptor fluorescence. BODIPY-FL acceptor emission from the labelled wildtype protein is indicated (*green arrow*).

(E) Luminescence decay of the indicated $STIM1^{CT}$ proteins, followed at the donor wavelength in the absence and presence of acceptor (τ_D, τ_{DA}) and at the acceptor wavelength (τ_{AD}). Acceptor decays correspond well to donor decays, except that the 0.21-ms component accounts for a larger fraction of the total amplitude. This difference is expected. The physical basis for the exaggeration of the rapid component in acceptor decay traces has been detailed in[59]. Residuals indicate no systematic deviation of the data from the fitted curves.

(F) Cartoon interpreting the results of panels 2D and 2E. The distance measured between residues 233 and 686 implies that the wildtype protein is folded back, whereas the “activated” L251S protein is extended.

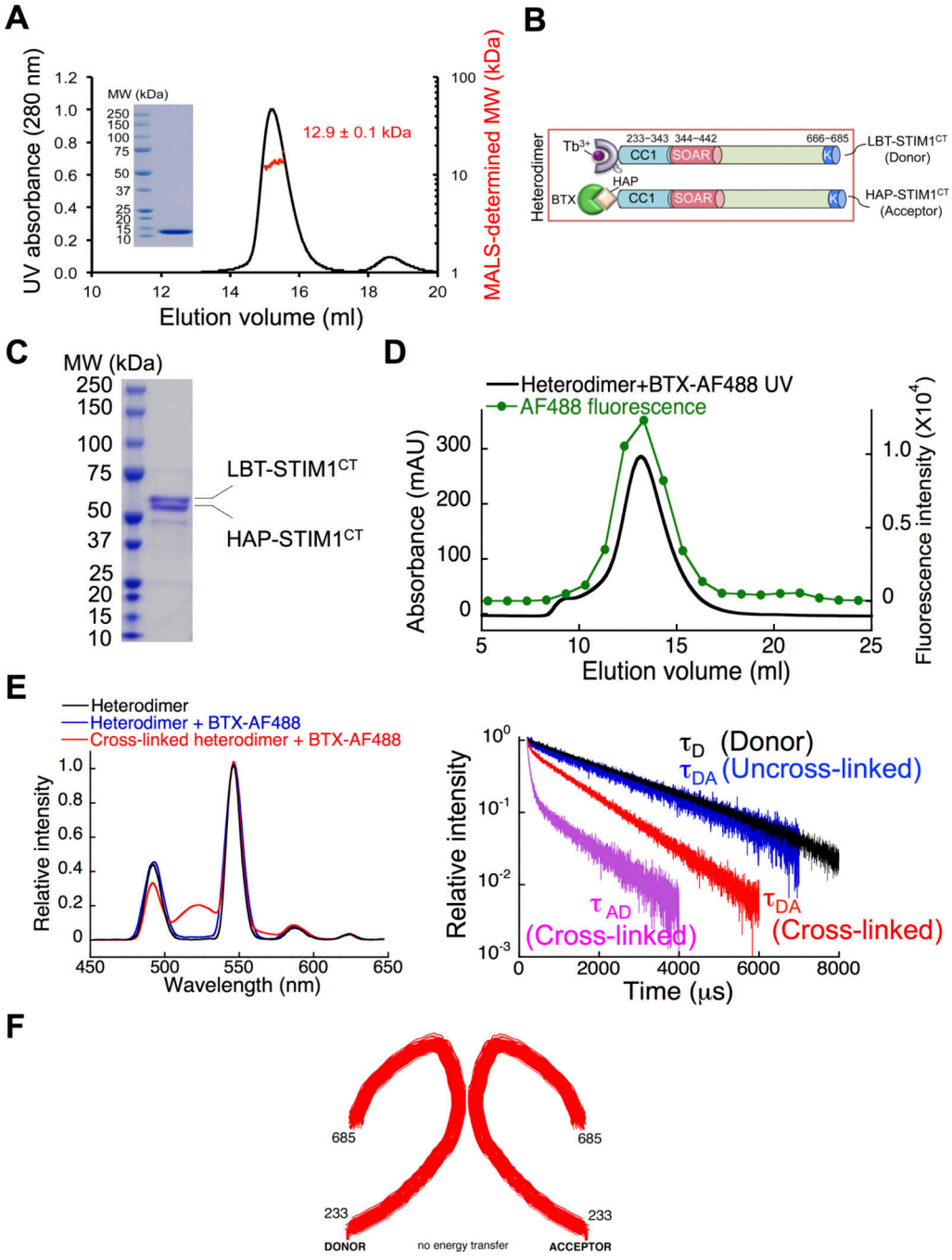

Figure 3. Lack of detectable CC1–CC1 association

(A) Recombinant CC1 is monomeric. SEC-MALS determination of CC1 molecular mass (*right axis*) is plotted with the UV absorbance trace indicating the protein peak (*left axis*). *Inset*, SDS-polyacrylamide gel analysis of the purified CC1 protein.

(B) Schematic of STIM1^{CT} heterodimer in which one monomer was tagged at its N terminus with an LBT and the other monomer with a HAP peptide that binds the 8 kDa ligand α-bungarotoxin (BTX) with high affinity. The introduced cysteine residues used to crosslink the N termini are not shown.

(C) SDS-polyacrylamide gel analysis, documenting that the heterodimer, as prepared, has roughly equal amounts of LBT-STIM1^{CT} and HAP-STIM1^{CT}.
(D) Size-exclusion chromatography shows that bound fluorescent α-bungarotoxin forms a stable complex with STIM1^{CT} protein. The UV absorbance signal from protein (*black curve* and *left axis*) and the fluorescence signal from Alexa Fluor 488-labelled α-bungarotoxin in fractions eluting from the column (*green symbols* and *right axis*) are plotted against elution volume.
(E) CC1 regions are not associated in dimeric STIM1^{CT}*Left*, gated fluorescence spectra of the heterodimer with Tb^{3+} donor alone (*black*), uncrosslinked heterodimer with Tb^{3+} donor and fluorescent α-bungarotoxin acceptor (*green*), and N-terminally crosslinked heterodimer with Tb^{3+} donor and fluorescent α-bungarotoxin acceptor (*red*). *Right*, corresponding luminescence decay curves. Tb^{3+} donor emission was monitored except in the case labelled τ_{AD}, for which acceptor emission was monitored. Energy transfer between Tb^{3+} and fluorescent α-bungarotoxin was observed when the N termini of the heterodimer were artificially apposed by forming a disulfide link, verifying that the assay detects CC1–CC1 proximity. However, there was no intradimer energy transfer in the absence of crosslinking.
(F) Cartoon illustrating the conclusion that the N termini of the individual STIM1^{CT} monomers are not in close proximity in the STIM1^{CT} dimer.

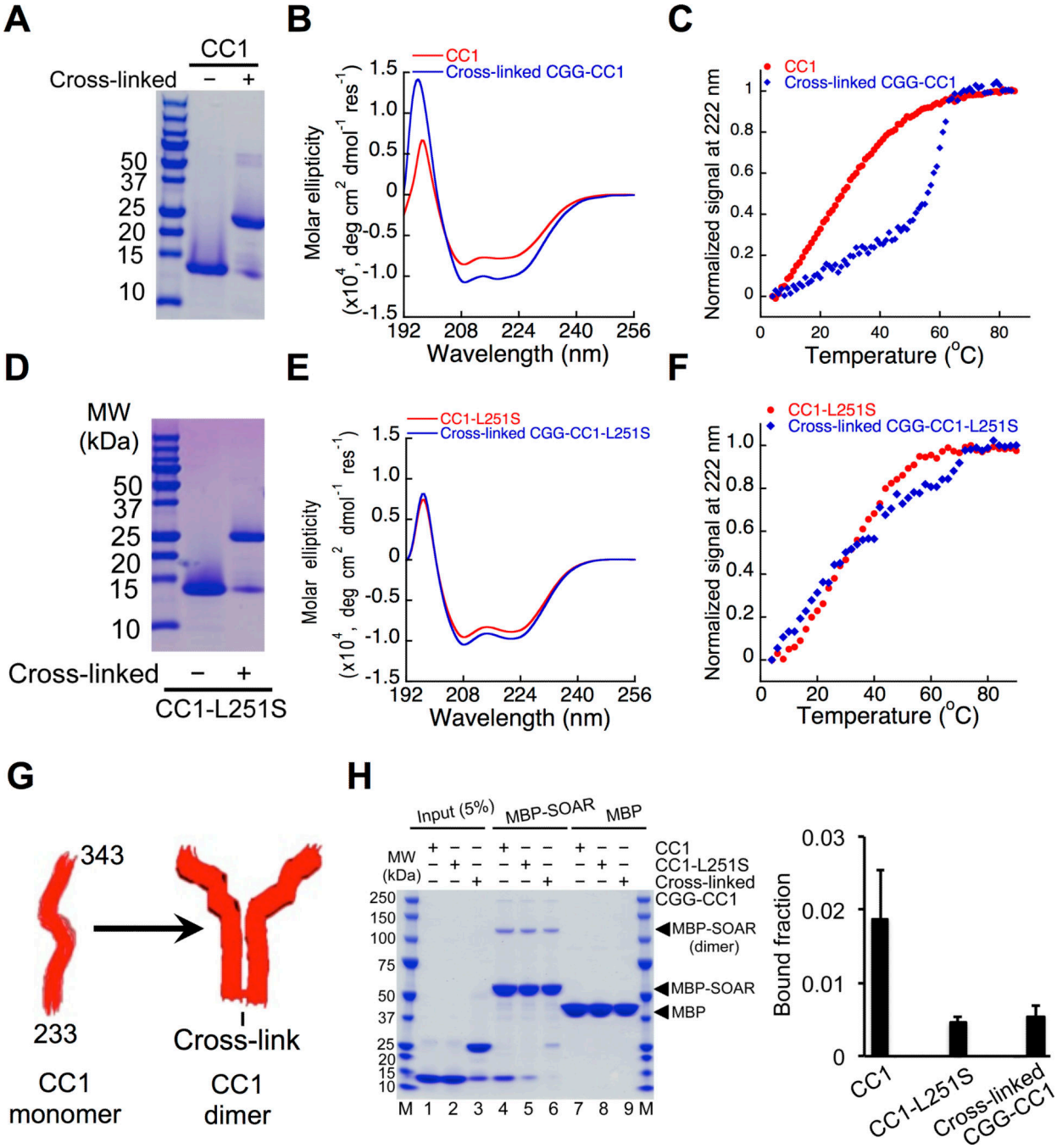

Figure 4. Effects of forced CC1–CC1 association

(A) Nonreducing SDS-polyacrylamide gel verifying efficient disulfide crosslinking of CC1.

(B) Far-UV CD spectra of uncrosslinked and crosslinked CC1. The dimer shows a modest increase in α-helix content, evident in the change in molar ellipticity at 208 nm and 222 nm.

(C) Thermal melting of CC1 and crosslinked CC1 monitored at 222 nm. The dimer shows pronounced stabilization of a part of its α-helical structure.

(D) Nonreducing SDS-polyacrylamide gel verifying efficient disulfide crosslinking of CC1(L251S).

(E) Far-UV CD spectra of uncrosslinked and crosslinked CC1(L251S). The disulfide-linked CC1(L251S) dimer shows little change in α-helix content.
(F) Thermal melting of CC1(L251S) and crosslinked CC1(L251S) monitored at 222 nm. In contrast to the finding with wildtype CC1 (panel 3D), disulfide crosslinking fails to stabilize the secondary structure of CC1(L251S).
(G) Cartoon of CC1 as the monomer or as the disulfide-linked dimer. A straightforward interpretation of the differing results in panels 3D and 3G is that the increase in α-helix content and the stabilization of secondary structure occurs as a result of coiled coil formation adjacent to the site of crosslinking,
(H) Binding of CC1, CC1(L251S), and crosslinked dimeric CC1 to immobilized MBP-SOAR. *Left*, the indicated samples were analyzed on a nonreducing SDS-polyacrylamide gel. Representative of three experiments for CC1 and dimeric CGG-CC1, and two experiments for CC1(L251S). *Right*, quantitation of the fraction of CC1 bound to MBP-SOAR.

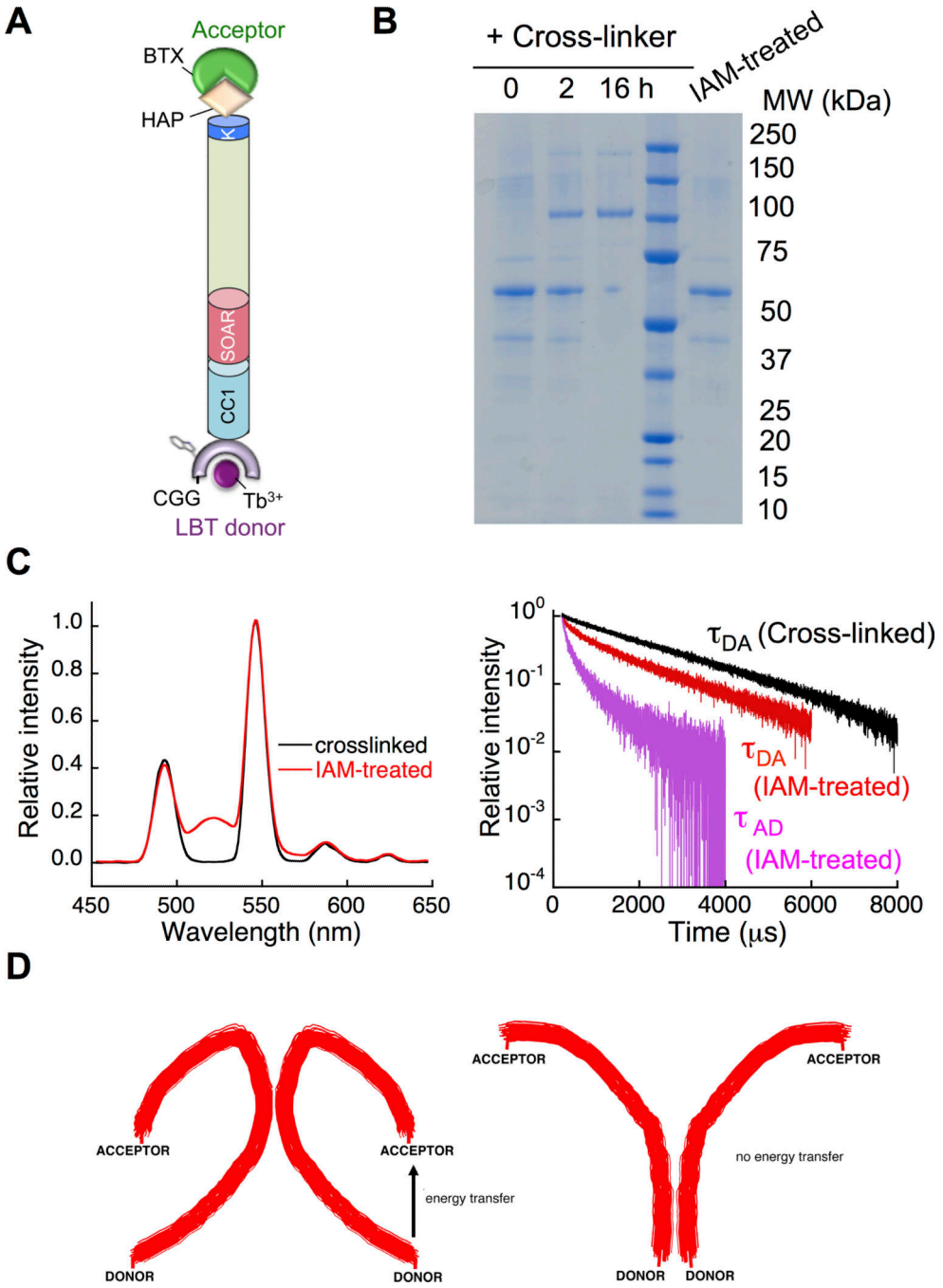

Figure 5. Intradimer CC1–CC1 association triggers extension of the STIM1 cytoplasmic domain

(A) Schematic illustrating the placement of labels, with an LBT binding Tb^{3+} at the N terminus of $STIM1^{CT}$ and a HAP tag binding Alexa Fluor 488-labelled α-bungarotoxin at the C terminus. To allow crosslinking in this experiment, a cysteine residue was introduced at the extreme N terminus of $STIM1^{CT}$.

(B) Reducing SDS-polyacrylamide gel documenting the effectiveness of crosslinking after a 16-h reaction.

(C) CC1–CC1 crosslinking abolishes energy transfer between N-terminal donor and C-terminal acceptor. *Left*, gated fluorescence spectra of the iodoacetamide-blocked (*red*) and crosslinked (*black*) samples. *Right*, corresponding luminescence decay curves. Tb^{3+} donor emission was monitored except in the trace labelled τ_{AD} (*green*), for which acceptor emission was monitored.

(D) Cartoon interpreting the results of panel 5C. CC1–CC1 crosslinking, like the L251S mutation, leads to an extended conformation of $STIM1^{CT}$.

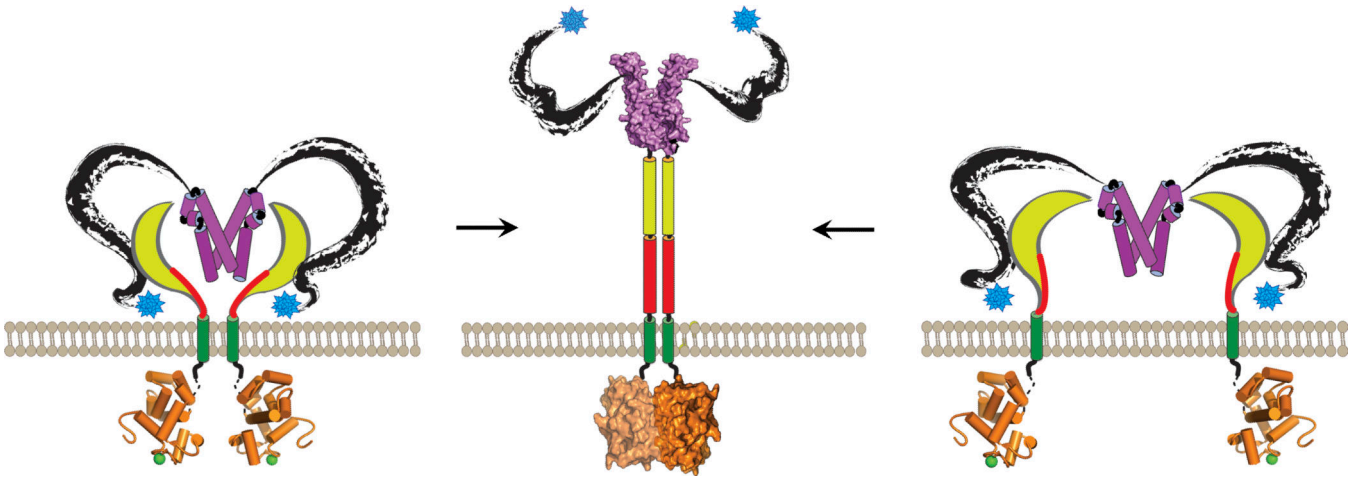

Figure 6. Model for STIM1 activation in cells

Left, inactive STIM1, with the individual CC1 regions (*red* and *yellow*) interacting with the SOAR(CAD) domains (*magenta*) (Figure 4H), a relatively short distance between the N terminus of CC1 and the STIM1 C-terminal polybasic tail (*blue*) (Figure 2D–E), and the polybasic tail partially buried (Figure 1D). STIM1 ER-luminal domain (*brown*) and SOAR(CAD) structures are as reported in the literature[16,53]. Detailed structural information for CC1 and for the region (*black*) C-terminal to SOAR(CAD) is not available. The model is not intended to specify the configuration of the polypeptide backbone that links CC1 to SOAR(CAD), or the surface(s) of SOAR(CAD) that are in contact with CC1. *Right*, an alternative possibility for inactive STIM1, with the N termini of its two CC1 segments separated (Figure 3E). Note that if L251 and SOAR(CAD) interact directly (Figure 4H), the geometry of SOAR(CAD) in this case is likely to differ from that of the crystallized domain depicted. *Center*, active STIM1, with the initial portions of CC1 (*red*) coming together in a coiled coil (Figure 4A–F), a loss of the CC1–SOAR(CAD) interaction (Figure 4H), and an increased distance between the N terminus of CC1 and the polybasic tail (Figure 5C). The structures of the luminal domain and of SOAR(CAD), rendered as solid dimers in active STIM1, have not been determined.

Table 1

A LRET distance estimates

Protein	Donor–acceptor pair	R_0 (Å)	Donor emission at 490 nm or 545 nm			Acceptor emission at 515 nm or 570 nm		
			τ_{DA} (μs)	E	R (Å)	τ_{AD} (μs)	E	R (Å)
WT	Tb^{3+}–BODIPY_FL	44.0	277 (32%) 1214 (41%) 2317 (27%)	0.88 0.48	31.5 44.7	206 (40%) 977 (60%)	0.91 0.58	29.8 41.7
	Tb^{3+}–BODIPY_TMR	54.3	189 (27%) 836 (32%) 2359 (41%)	0.92 0.64	36.3 49.3	189 (44%) 941 (56%)	0.92 0.59	36.3 50.7
	Tb^{3+}–GFP	44.1	189 (29 %) 1036 (42 %) 2329 (29 %)	0.92 0.55	29.6 42.6	311 (15 %) 1081 (85 %)	0.87 0.53	32.3 43.1
L251S	Tb^{3+}–BODIPY_FL	44.0	2167 (100%)	[0.066]	[68.4]	negligible acceptor emission		
	Tb^{3+}–BODIPY_TMR	54.3	2208 (100%)	[0.048]	[89.2]	negligible acceptor emission		
	Tb^{3+}–GFP	44.1	2164 (100%)	[0.067]	[68.4]	negligible acceptor emission		

B LRET distance / conformational change parameters

Protein	Donor–acceptor pair	R_0 (Å)	From donor emission					From acceptor emission				
			τ_1 (μs)	E	R (Å)	τ_{ex} (μs)	F	τ_1 (μs)	E	R (Å)	τ_{ex} (μs)	F
WT	Tb^{3+}–BODIPY_FL	44.0	309	0.87	32.3	1309	0.58	238	0.90	30.7	806	0.56
	Tb^{3+}–BODIPY_TMR	54.3	215	0.91	37.2	716	0.63	213	0.91	37.1	820	0.59

The data have been fitted to a model in which energy transfer reports on two populations of $STIM1^{CT}$ with distinct Tb^{3+}–acceptor distances.

Tabulated values of τ_{DA} and τ_{AD} are the average of values from three experiments. Data from the individual experiments are listed in Supplementary Table 1.

Amplitudes (%) of τ_{DA} and τ_{AD} have been corrected to zero time, and τ_{AD} has been corrected for energy transfer rate as in[59].

All energy transfer efficiency and distance calculations are based on τ_D = 2.32 ms.

E is the efficiency of Tb^{3+}–acceptor energy transfer.

R is the corresponding Tb^{3+}–acceptor distance.

Bracketed values [] are outside the range for accurate estimation.

The same data have been fitted to a model in which $STIM1^{CT}$ has two states, a folded-back state in which energy transfer occurs, and an extended state in which there is no energy transfer. The folded-back state extends with rate constant α, and the extended state folds back with rate constant β.

Calculations are based on τ_D = 2.3 ms

τ_1 is the lifetime $(k_{transfer} + k_{Tb})^{-1}$ for luminescence emission from the folded-back state of $STIM1^{CT}$.

E is the efficiency of Tb^{3+}–acceptor energy transfer in the folded-back state.

R is the corresponding Tb^{3+}–acceptor distance.

τ_{ex} is the characteristic time $(\alpha + \beta)^{-1}$ for exchange between the folded-back and extended states of $STIM1^{CT}$.

F is the fraction of $STIM1^{CT}$ in the folded-back state.